LUND UNIVERSITY

Wideband SIW-based Low-cost Multi-layer Slot Antenna Array for E-Band Applications

Aliakbari Abar, Hanieh; Mosalanejad, Mohammad ; Soens, Charlotte ; Vandenbosch, Guy A. E. ; Lau, Buon Kiong

LUND UNIVERSITY

PO Box 117
221 00 Lund
+46 46-222 00 00

Wideband SIW-based Low-cost Multi-layer Slot Antenna Array for *E*-Band Applications

Hanieh Aliakbari, *Graduate Student Member, IEEE*, Mohammad Mosalanejad, *Student Member, IEEE*, Charlotte Soens, Guy A. E. Vandenbosch*, Fellow, IEEE*, and Buon Kiong Lau, *Senior Member, IEEE*

Abstract—This paper proposes a substrate integrated waveguide (SIW) slot antenna array for wideband gigabyte mobile radio application in *E*-band. The wideband unit cell design is based on simultaneous feeding of 4-element radiation slots with a higher order cavity mode directly excited by a simple slot aperture fed by a microstrip fork-like tuning stub. Employing the higher order mode along with the slot aperture facilitate low loss, simple feeding network and lower sensitivity to fabrication errors. To cancel the beam tilt versus frequency, the higher order mode unit cell is used in a 2 × 2 array along with a differential feeding structure. The array was designed and taped out using a new high-resolution multi-layer PCB technology and characterized by using the constructed millimeter wave measurement setup at KU Leuven /IMEC. This technology provides the possibility to stack micro-vias in PCB boards and reduce fabrication cost compared to other multi-layer technologies in mm-wave bands. The proposed array in 2 × 2 array configuration has a measured bandwidth of 11.4 GHz (16%), a total efficiency of 69%, a realized gain of 12 dBi at 72 GHz and a 3-dB gain bandwidth that covers the entire impedance bandwidth. In comparison to existing *E*-band SIW slot arrays (compensating for array sizes), the proposed design achieves similar or better performance in bandwidth but with lower cost, lower sensitivity to fabrication tolerances and higher total efficiency.

Index Terms— Advanced multi-layer PCB, differential-fed antenna array, *E*-band, SIW cavity higher order mode.

I. INTRODUCTION

DUE to the large available bandwidth, a broad range of applications are rapidly emerging in millimeter wave (mm-wave) bands [1]. In particular, the first implementable fifth-generation (5G) standard for mobile communications, i.e., 5G New Radio (NR), includes the use of mm-wave to deliver robust mobile broadband access [2]. Furthermore, for the higher part of mm-wave bands, ITU has allocated

unlicensed/lightly-licensed spectra in the 60/70/80 GHz bands, intended for a number of applications such as fixed cellular backhaul links, broadband local area networks (LANs) and potential 5G systems with multi-gigabyte data rate [3]. One important criterion to ensure marketplace adoption of wireless systems in this band is the availability of low-cost and mass-producible antennas.

Recently, CMOS technology capable of low-cost mass production is introduced for mm-wave transceiver implementation. Thus, the practical realization of an antenna array for mm-wave relies on a suitable interface between the active circuits and the antenna, and it is important to choose an antenna fabrication technology that is easy to integrate with mm-wave integrated silicon transceiver. Smaller dimensions of antennas in *E*-band than the conventional 60 GHz or lower bands allow the antennas to be comparable in size with the active circuit blocks (e.g., processor, memory and radio). This has led to on-chip antennas (OCAs) on standard silicon substrates [4], [5] to eliminate the need for a circuit-antenna interface. However, these antennas do not work very well (e.g., ~ -8.5dBi gain at 79 GHz [5]) because of the high permittivity (~11.7) and low-resistivity (~10 Ω.cm) of silicon substrate. Other main *E*-band antenna fabrication technologies are low temperature co-fired ceramic (LTCC), liquid crystal polymer (LCP) and printed circuit boards (PCBs) [6]. The LTCC technology has more design freedom with via placement and tight tolerance. However, antenna in package (AIP) on LTCC substrate is less attractive in *E*-band because of its high cost and considerable loss caused by the relatively high dielectric constant of the LTCC substrate [7]. Although LCP [8] is cheaper than LTCC, both of them have long production cycle. On the other hand, for the conventional PCB technology, the minimum spacing and diameter of the machine drilled vias are electrically large in *E*-band and the impact of fabrication errors becomes more severe. The above considerations motivate the urgent need for a new or improved *E*-band antenna technology that is both low cost and low loss.

In the higher part of mm-wave bands, substrate integrated waveguide (SIW) has become a key technology in the realization of antennas. This is because it has the advantages of rectangular waveguide features, such as lower loss in mm-wave and ease of connection to active components and coplanar waveguide (CPW) lines. Several SIW-based antenna structures have been proposed for *E*-band [3], [8]-[14]. In [9],
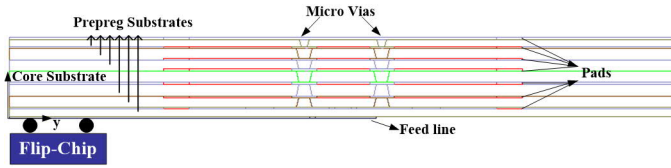
Fig. 1. Schematic of an advanced multi-layer PCB technology connected to the monolithic microwave integrated circuit (MMIC) for system-level assembly by solder bump flip-chip technology.

longitudinal slots are utilized to feed circular patches. However, the used resonant feeding technique leads to a narrow bandwidth. On the other hand, the SIW-fed antipodal linearly tapered slot antenna in [8] has a large operating bandwidth, but its end-fire radiation characteristic limits its application in wireless communications, since broadside radiation pattern is often required. Moreover, the proposed design cannot be extended for planar 2D array application. In [10], the fundamental cavity mode is used in the proposed 8×8 slot array, resulting in a substantial insertion loss (~3 dB) of the mode excitation feeding network at 60 GHz. In the same way, the 4×4 slot array reported in [12] provides low total efficiency in E-band (i.e. ~38%) because of the use of a large and lossy feeding network. A more simplified antenna feeding network is reported for the fundamental mode cavity in [11] and all resonant cavities are connected with inductive windows. However, the achieved bandwidth, considering both gain and impedance, is relatively small (i.e., ~10%) [3], [13], [14].

In comparison with arrays that utilize the fundamental cavity mode, arrays that utilize higher order mode(s) can provide simpler feeding structure. Most existing SIW antennas that utilize higher order mode(s) are designed for lower bands [15]-[17]. However, the feeding network used for the excitation of the mode is still complex in [15] and the impedance bandwidth is small (~5.5%). In addition, the direct excitation probe feed used in [16], [17] is not suitable for integration with active circuits in higher mm-wave bands.

This work focuses on the design and implementation of wideband and simple-feed SIW slot antenna array suitable for E-band applications by using an advanced low-cost PCB technology. To realize boresight radiation and simple feed in the unit cell, two parallel higher-order mode resonant cavities are simultaneously excited in a wide bandwidth, only by a slot aperture and a modified 50Ω line. Aperture excitation is utilized rather than direct feed for better circuit integration in this frequency band. Using the TE$_{201}$ mode in the unit cell simplifies the lossy power divider network in larger slot array design and also reduces the number of SIW metal posts, which reduces metal loss and fabrication cost in E-band. Moreover, using TE$_{201}$ facilitates relaxed fabrication tolerance and higher accuracy, leading to enhanced stability in performance, properties that are more important in E-band than lower frequencies. A differential feeding network is also designed and utilized to mitigate the beam deviation problem in [16]. The measured results of the fabricated unit cell and 2×2 array in mm-wave measurement setup agree well with the full-wave simulation results.

TABLE I
PROPERTIES SPECIFICATIONS OF THE "ANY-LAYER HDI PCB TECHNOLOGY"

Material	Dielectric constant	Tangent delta	Thickness (um)
Copper 8 (cavity bottom layer)			23
Sub7: Prepreg Substrate (metal post)	3.26	0.006	60
Copper 7 (internal plane 3)			16
Sub6: Prepreg Substrate (metal post)	3.22	0.006	104
Copper 6 (Signal)			16
Sub5: Prepreg Substrate (metal post)	3.22	0.006	104
Copper 5 (Signal)			23
Sub4: Laminate core Substrate (metal post)	3.37	0.006	100
Copper 4 (internal plane 2)			23
Sub3: Prepreg Substrate (metal post)	3.22	0.006	104
Copper 3 (Signal)			16
Sub2: Prepreg Substrate (metal post)	3.22	0.006	104
Copper 2 (internal plane 1 and slots)			16
Sub1: Prepreg Substrate	3.25	0.006	60
Copper 1 (modified microstrip line)			23

II. ADVANCED MULTI-LAYER PCB TECHNOLOGY

A PCB with 8-layer stack-up, as shown in Fig. 1, is used in this work. This stack-up has 7 Panasonic Megtron 6 substrates [18] and 8 metal layers, with the properties listed in Table I. The substrate properties were characterized by measurement at 50 GHz. To the authors' knowledge, these measured properties are the closest available in frequency to the E-band. Internal planes 1, 2 and 3 are ground planes and others are signal planes. This PCB technology is called "*Any-Layer HDI (High Definition Interconnect) PCB technology*", and it is the most advanced PCB technology in the world, with very high resolution down to 40μm line width [19].

The "*Any-Layer HDI PCB technology*" is an improvement of the standard multi-layer PCB technology [20], which is significantly more cost-effective than LTCC. In this technology, laser-drilled stacked micro-vias are used instead of machine drilled vias in standard PCB technology, for all electrical connections between the two non-stacked metal layers in Fig. 1. In general, conventionally blind or through holes are replaced by copper filled micro-vias of significantly smaller dimensions: the minimum hole and pad size of machine drilled vias are 200um and 400um, while for laser drilled micro-vias are 75um and 175um. This means that each layer or connection on a specific layer can be connected with every other layer within the PCB stack-up without using big via holes, resulting in space saving and increased routing density for a given product dimension. The pad sizes are 0.23 mm. Micro-vias are cone shaped (see Figs. 1 and 3(a)) with approximate large and small diameters of 0.075-0.14 mm and 0.055-0.1mm, respectively. The steps of the fabrication process are summarized in Fig. 2 [21]. The process starts with the core layer (i.e., 4th layer in Table I). The "prepreg" substrates work as glue to paste substrates together, so first they are cured (melted), and then they are laminated on the previous laminated substrates. After curing (when the prepreg substrates become cold), then substrates are ready for the mapping of metal routes or the making of laser-drilled micro-vias through them.

This technology has a high resolution close to LTCC and can be used for mm-wave applications up to 100 GHz. Since this technology has lower tape-out cost and fewer fabrication difficulties than other technologies at mm-wave bands
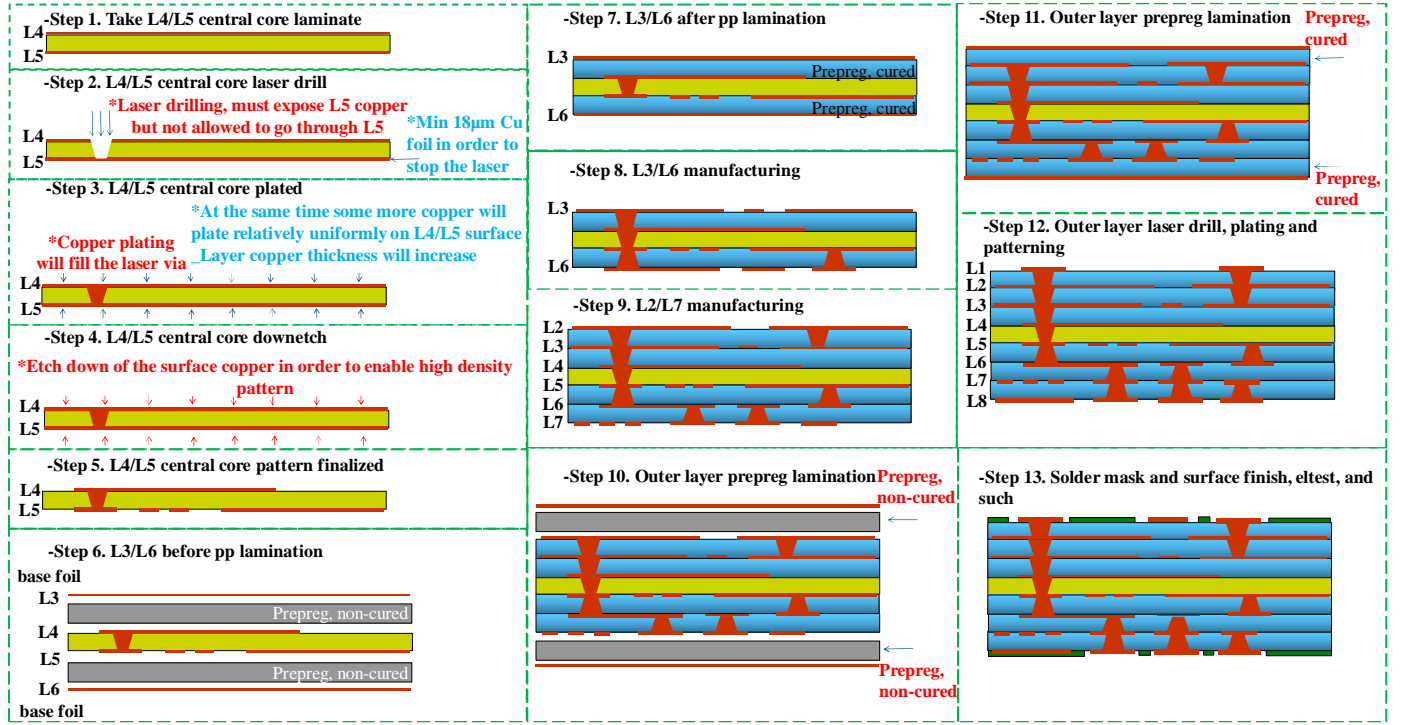
Fig. 2. 13 steps in fabrication process of "*Any-Layer PCB Technology*" [21].

(e.g., LTCC, LCP), it is attracting significant interest in the industry

III. CAVITY BACKED UNIT CELL DESIGN

Figures 3(a) and 3(b) show the simulated electric field (E-field) and magnetic field (H-field) distribution along the YZ and XY cross sections of a cavity operating in the TE_{201} mode, respectively. The simulation was performed with Ansys HFSS 15's finite element solver. The XZ-plane of the cavity in Fig. 3 can be considered as a virtual ground plane and the cavity is separated into two independent cavities. According to the waveguide theory [22], the resonant frequency of the TE_{201} mode in the aforementioned resonant cavity is

$$f_{TE_{201}} = \frac{ck_{TE_{201}}}{2\pi\sqrt{\mu_r\varepsilon_r}} = \frac{c}{2\pi\sqrt{\mu_r\varepsilon_r}}\sqrt{\left(\frac{2\pi}{L}\right)^2 + \left(\frac{\pi}{W}\right)^2} \quad (1)$$

where μ_r and ε_r are the equivalent relative permeability and permittivity of one multi-layer cavity substrate, respectively. c is the speed of light and k_{TE201} is the effective wave number. L and W are the length and the width of the corresponding resonant cavity in Fig. 3. The field distribution of TE_{201} mode in the cavity is given by [22]

$$E_x = E_y = H_z = 0 \quad (2)$$
$$E_z = E_0\sin(2\pi y/L).\sin(\pi x/W) \quad (3)$$
$$H_x = j\pi E_0/k\eta L.\cos(2\pi y/L).\sin(\pi x/W) \quad (4)$$
$$H_y = -jE_0/Z_{TE}.\sin(2\pi y/L).\cos(\pi x/W) \quad (5)$$

which show that the fields in the cavity form standing waves. E_0 is the amplitude constant. When two slots are approximately etched on top of the TE_{201} mode resonant cavity as shown in

Fig. 3(b), one elementary unit cell (of 1×2 slot elements) can be realized without the need for any power divider to individually feed the independent cavities. Based on this principle, two parallel TE_{201} mode resonant cavities and four slots is embedded in the stack-up of Fig. 1 and the resulting antenna can be regarded as a new unit cell consisting of two side-by-side 1×2 slot array, 1-D antenna unit cells on the YZ-plane. The layout of the 4-element slot antenna (one-unit cell) is illustrated in Fig. 4. Here the effective length/width (i.e., L_{cavity} /W_{cavity}) of the whole resonant cavity is chosen to be one guided wavelength of the resonant frequency (= $c/(f_{TE_{201}}\sqrt{\mu_r\varepsilon_r})$) to support the TE_{201} mode in each resonant cavity. As depicted in Fig. 4(a), the input microstrip line is etched on the first copper layer of the PCB in Table I whereas the first internal plane forms the ground plane. The higher
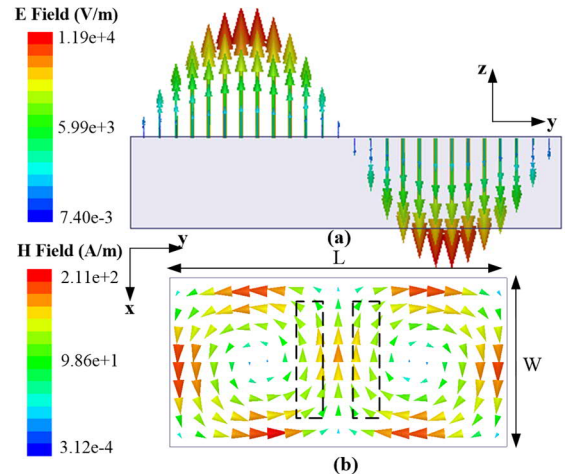

Fig. 3. (a) E-field and (b) H-field distribution of the TE_{201} mode, along YZ and XY cross sections of the cavity as an elementary unit cell, respectively.
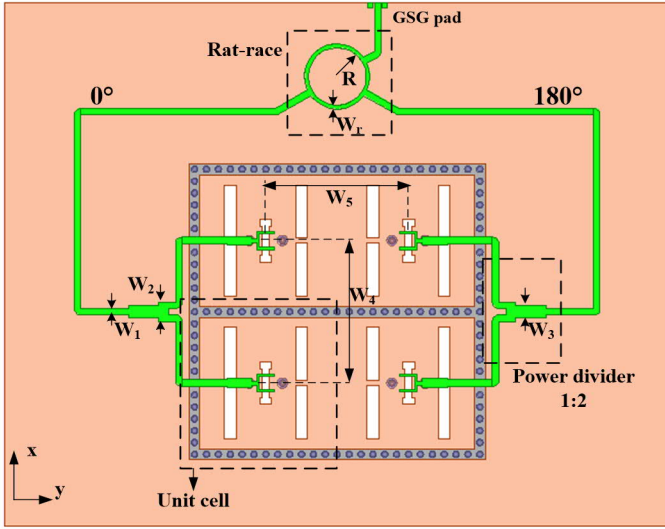
Fig. 4. Unit cell slot antenna structure comprised of two parallel TE_{201} resonant cavities shown in (a) perspective view and (b) top view with design parameters. The corresponding layers are listed in Table I.

Fig. 5. (a) E-field magnitude distribution and (b) current vector distribution at 73 GHz. (For clarity only internal plane 1 is shown.)

Fig. 6. (a) Simulated S_{11} of the unit cell with two stacked micro-vias in comparison with machine drilled vias, (b) impact of different R_2 on S_{11} in the Smith chart over 71-76 GHz.

order mode resonant cavity is located at the top of the internal plane 1 and the cavity's side walls are formed by rows of stacked micro-vias between the internal plane 1 and copper 8 layer. It is noteworthy that by using the cavity micro-vias in Fig. 3(a), the resulting TE_{201} mode is not as perfect as the cavity with solid planes, especially at higher frequencies, thus (1)-(3) offer only approximations of the real values.

A small H-shaped coupling slot aperture is cut at the center of the internal plane 1, which effectively couples the energy from the modified microstrip line to the cavity. In this way the two parallel TE_{201} resonant cavities are simultaneously excited by the single-slot aperture without the need for any complex power divider to individually feed the four radiating resonant slots. In order to improve the front to back ratio (FTBR) of the array, the resonant slots are located on the same side with the aperture coupling slot [23]. The antenna is fed by a 50-ohm microstrip line followed by a fork-shaped feeding structure, positioned symmetrically with respect to the centerline of the YZ-plane. The fork-shaped feed comprises of one horizontal and two vertical stubs, which realizes more effective coupling with the slot for achieving bandwidth enhancement [24].

Two metal posts including cone shaped stacked micro-vias are introduced on both sides of the coupling slot in Fig. 4(a) for splitting the electromagnetic (EM) power between the slots and improving the impedance matching. As shown in Fig. 5(a), the EM energy is coupled from the fork-shaped line, split in to two parts by the H-slot aperture, and fed into the TE_{201} mode of the multi-layer cavity. Figure 5(b) shows that the radiation slots are excited in phase since the directions of the current flow at the two sides of each slot are identical and in this way broadside radiation can be achieved.

To show the importance of the small stacked micro-vias provided by the "*Any-Layer HDI PCB technology*" in our design, the matching stacked micro-vias in the middle of the unit cell cavity were replaced by machine drilled vias in conventional PCB technology (i.e. with double hole and pad size compared to micro-vias as indicated in Section II), and the achieved results are compared in Fig. 6. The impedance bandwidth of the unit cell and the locus of S_{11} on the Smith chart and are illustrated in Fig. 6(a) and 6(b), respectively. As can be seen in Fig. 6(b), smaller micro-vias (i.e. parameters of R_1 and R_2 in Fig. 4) are important to achieve a larger input impedance bandwidth. It can be observed that by making the micro-via diameter wider and wider (i.e. close to machine drilled vias in conventional PCB technology), the corresponding locus gets farther and farther away from the center of the Smith chart. Furthermore, as a result of the larger vias the electromagnetic field in the cavity will be disrupted and the radiation pattern will be changed significantly in the band of operation.

Moreover, the minimum distance between machine drilled vias in conventional PCB process are two times the distance between stacked micro-vias in "*Any-Layer HDI PCB technology*", which by itself makes the performance of the SIW cavity more non-ideal, which can lead to worse results. However, for the proof of concept, we have just demonstrated the negative effects of applying machine drilled vias instead of micro-via matching sets in Figs. 6.

IV. DIFFERENTIALLY-FED SLOT ANTENNA ARRAY

The higher order mode unit cell in Fig. 4 can be arranged to

Fig. 7. Schematic of the differential-fed slot antenna array. The dimensions are: L_{cavity}= 3 mm, W_{cavity}= 3.25 mm, $L_{S1} = L_{S2}$ = 1.12 mm, $D_1 = D_2$ = 0.75 mm, W_{SF} = 0.25 mm, L_{SF} = 0.9 mm, $W_{S1} = W_{S2}$ = 0.2 mm, W_{pitch}= 0.25 mm, W_{PAD} = 0.23 mm, W_{F1} = 0.14 mm, W_{F2} = 0.18 mm, W_{F3} = 0.05 mm, L_{F2} = 0.575 mm, L_{F3} = 0.370 mm, L_{F4} = 0.4 mm, W_r = 0.08 mm, R = 0.61 mm, W_1 = 0.14 mm, W_2 = 0.41 mm, W_3 = 0.25 mm, $W_4 = W_5$ = 3 mm, R_1 = 0.085 mm, R_2 = 0.14 mm.

Fig. 8. (a) Bottom view of fabricated multi-layer antenna unit cell and (b) 2 × 2 array with advanced PCB technology, (c) constructed on-probe antenna measurement system.

realize a larger array of 2×2 unit cells with higher gain and a simple feeding network (see Fig. 7). In an ideal case, the E-field in the cavity is antisymmetric about the XZ-plane in the unit cell and symmetric about YZ-plane (see Fig. 3(b)). In practice, especially due to the non-ideal antenna setup, such as the use of micro-vias instead of solid plane in the cavity and the placing of feed line on top of the slot unit cell shown in Fig. 4, the E-field in the cavity is not fully symmetric especially in wide mm-wave bands. Thus, the excited E-field and voltage in the slots are not exactly the same, which leads to far-field beam tilts within the large operating bandwidth, particularly in the YZ-plane. Similarly, beam deviation will be even more severe if a higher order cavity mode (TE401) is excited to allow the 2×2 unit cells to be replaced by a single unit cell with a single feed. To avoid any beam tilt during frequency scanning of the slot array in Fig. 7, one side of the array is fed with an in-phase signal, whereas the opposite side of the array is fed with the same signal but shifted in phase by 180°. This differential feeding method can be easily integrated with differential devices, and it also improves cross polarization [25]. To form the two feeding signals, two T-junction power dividers and a modified rat-race coupler is designed and connected to the fork-like stub in the first copper layer (see Fig. 7). In comparison with other feeding methods, this method does not need a resistive load which is actually problematic at mm-wave frequencies. A 150 μm pitch ground-signal-ground (GSG) pad is used to feed the rat-race. With the differential feeding, the symmetric plane of the cavity in Fig. 7 acts as a ground plane. Therefore, the micro-vias along the XZ-plane could be removed without affecting the field distribution. In order to have less interfere with slot radiations we can choose stripline type of feeding network instead of microstrip lines in Fig.7. However, the thickness of SIW cavity and consequently the bandwidth will be reduced by using
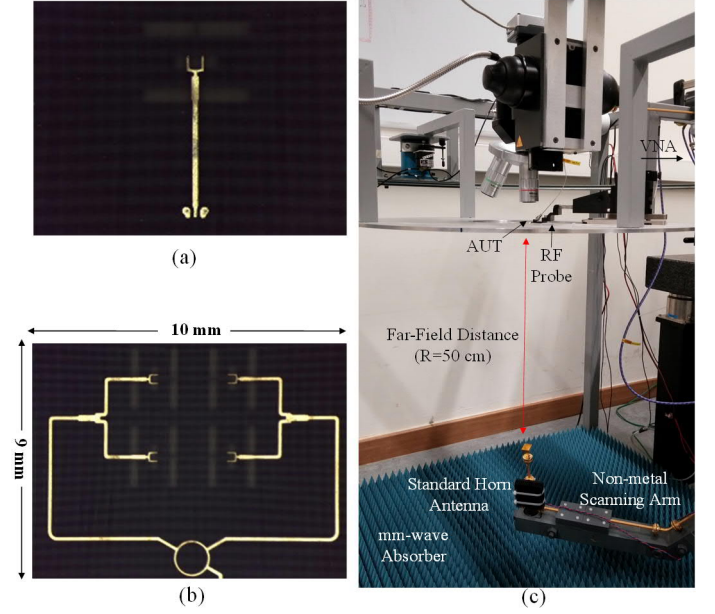
stripline feeding network in the inner layers of Table I. Moreover, stripline circuits have more loss than microstrip lines. For this reason, the microstrp line feeding network is proposed in Fig. 7. However, it does not change the generality of the concept which is the ability of the unit cell to be extended to larger differential-fed array structures.

V. SIMULATION AND MEASUREMENT RESULTS

One-unit cell slot antenna and one 2 × 2 array are designed and optimized in E-band using the finite element solver of Ansys HFSS 15. The operation frequency is higher than the characterization frequency in Table I. Therefore, to have more realistic results we have used loss tangent of 0.01 in the simulations. To check for possible emission at and around the fundamental mode, the performance of the unit cell was also simulated in the range 20-50 GHz. Poor matching is found in this lower frequency range; hence very little unwanted emission is expected. Each of the proposed antennas is etched on a multi-layer advanced PCB that provides low cost implementation for E-band applications. The multi-layer antenna prototypes are shown in Fig. 8(a) and (b). In the and proposed structure, a broadband microstrip-to-waveguide transition [26] is not needed for the measurement (see Fig. 1), unlike [10]-[13]. The main part of the mm-wave antenna measurement system is shown in Fig. 8(c). The functional frequency band of the constructed antenna mm-wave on-probe measurement setup is from 30 to 90 GHz [27]. A metal table that is suspended in the center is used as a holder for the micro-positioner and the probe. The on-probe antenna under test (AUT) is fixed in the center of the table. A scanning arm fabricated from a non-conducting material, such as PVC, is used to carry the horn antenna. The whole measurement system fits into a volume of about 1.5 m³.

The final antenna reflection coefficient is shown in Fig. 9.

TABLE II
COMPARISON AMONG SOME *E*-BAND SIW SLOT ARRAYS WITH BROADSIDE PATTERNS USING DIFFERENT TECHNOLOGIES

Ref.	f_0 (GHz)	No. of Unit cells and Feeding Method	BW (%)	GBW(%)	Gain (dBi)	TE(%)	Technology and Cost	Resolution
[3]	81.75	2×8-Open ended pentagonal array, power divider.	11.6	10	15	50	PCB, low	low
[10]	60	8×8 array, power divider.	17.1	17.1	22.1	44	LTCC, high	high
[12]	79	4×4 array, power divider.	10.7	6	11	38	Flexible PCB foil, low	high
[13]	60	12×12 array, power divider.	5	5	22	68	PCB, low	low
Proposed	73	Unit cell, direct aperture feed.	16.4	16	7.15	83	Any layer PCB, low	high
Proposed	72	2×2-unit cell array, differential aperture feed.	16	16	12	69	Any layer PCB, low	high
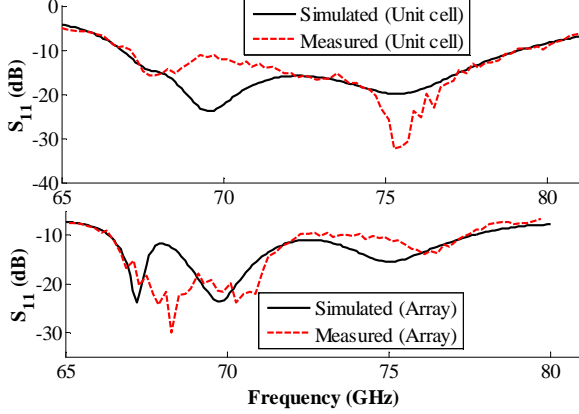
Fig. 9. Simulated and measured S_{11} of the slot antenna unit cell and 2 × 2 array.

Fig. 10. Radiation patterns of the antenna array in XZ (left) and YZ (right) plane at (a) 68 GHz, (b)73 GHz, (c)78 GHz. (cross polar is low in simulation).

The antenna unit cell and array exhibits a relatively large 10-dB impedance bandwidth from 67 to 79 GHz and from 66.3 to 77.7 GHz, respectively. It can be seen that reasonable agreement is achieved between measured and simulated results and they both give the same impedance bandwidth. The difference between them is mainly due to the tolerance of the thickness and permittivity of the materials. The radiation patterns are shown in Fig. 10 at three different frequencies within the bandwidth. As can be seen, broadside radiation is obtained in both XZ- and YZ-planes and the patterns has narrower beam in XZ-plane compared to the YZ-plane. The peak gain is 7.15 dBi and 12 dBi at the center frequency, for the unit cell and array, respectively. The cross polarization levels are below -18 dB in the YZ-plane and XZ-plane at the center frequency. It is noteworthy that this cross polarization level and the pattern ripples are normal in mm-wave measurements, and is not different from other works in the literature [8], [12]. Discrepancies in the radiation patterns between the simulation and measurement may be caused by fabrication tolerance, misalignment between the AUT and the standard horn. The total efficiencies of the unit cell and the slot array are 83% and 69%, respectively. The lower efficiency of the slot array is mainly due to feeding network loss. The total efficiency is increased to 78% when the differential feeding network is excluded and different phase shifts are applied directly from two separate feeding points. Moreover, thanks to the specific feeding scheme, the antenna's simulated FTBR is higher than 20 dB.

Finally, Table II compares the performance of some *E*-band SIW-based slot antennas in terms of feeding technique, 10-dB impedance bandwid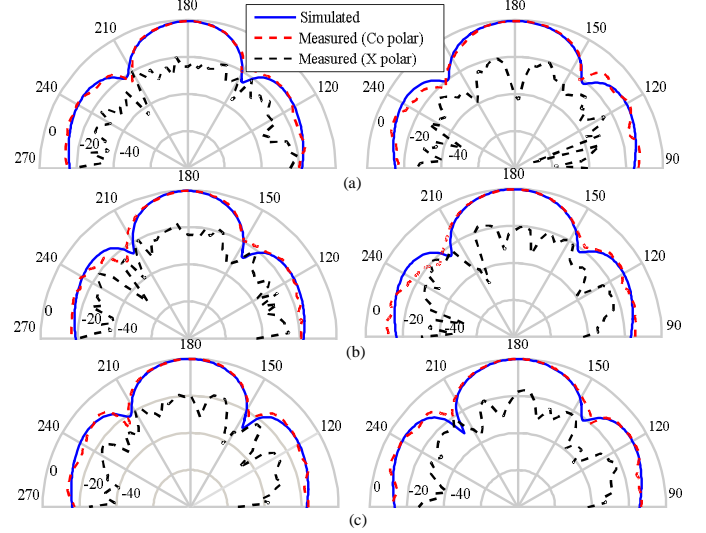th, 3-dB gain bandwidth (GBW), realized gain at the center frequency, total efficiency (TE), cost of technology, and resolution (i.e., fabrication accuracy). All the arrays in Table II (except [13]) offer 10% or more operating bandwidth. However, considering operating bandwidth, possibility for planar 2-D array application, cost and efficiency, this work gives the largest operating bandwidth in the targeted band. It is noteworthy about Table II that although series-fed slot array antenna in [12] has a thinner substrate, it suffers from large variation in gain (i.e. up to 11 dB) within the impedance bandwidth. In fact, the bandwidths of series-feed slot array antennas tend to decrease as the number of antenna elements increases [28].

VI. CONCLUSION

A 2 × 2-unit cell wideband differential-fed slot array is proposed in this work for *E*-band multi-Gbps applications. Based on the electric field properties of the higher order cavity mode, both the resonance cavity and the antenna feeding network for the unit cell can be realized efficiently, resulting in a simplified feeding network and relatively low loss in *E*-band. Moreover, the use of higher order mode makes the structure less sensitive to fabrication errors, desirable for *E*-band applications. A new and low-cost fabrication method with high accuracy (i.e., "*Any-Layer HDI PCB technology*") is used for the antenna realization. The antenna can be readily combined with active circuits (e.g., MMICs).

In summary, the proposed low-cost E- band SIW antenna array has the merits of simple feeding structure, wide

bandwidth, low loss and ease of integration with active circuits.

REFERENCES

[1] M. Marcus, and B. Pattan, "Millimeter wave propagation: spectrum management implications," *IEEE Microw. Mag.*, vol. 6, no. 2, pp. 54-62, Jun. 2005.

[2] 3GPP TS 38.101-2 v1.0.0 (2017-12). User Equipment (UE) Radio Transmission and Reception. Part 2: Range 2 Standalone (Release 15), 3GPP TSG RAN, NR, 2017.

[3] Z. Hao, M. He, K. Fan, and G. Luo, "A planar broadband antenna for the *E*-Band gigabyte wireless communication," *IEEE Trans. Microw. Theory Tech.,* vol. 65, no. 3, pp. 1369-1373, Mar. 2017.

[4] D. Hou, Y. Xiong, W. Goh, S. Hu, W. Hong, and M. Madihian, "130-GHz on-chip meander slot antennas with stacked dielectric resonators in standard CMOS technology," *IEEE Trans. Antennas Propag.,* vol. 60, no. 9, pp. 4102-4109, Sep. 2012.

[5] N. Demirel, Y. Pinto, C. Calvez, D. Titz, C. Luxey, C. Person, D. Gloria, D. Belot, D. Pache, and E. Kerhervé, "Codesign of a PA-antenna Block in silicon technology for 80-GHz radar application," *IEEE TransCircuits and Sys. II: Express Briefs*, vol. 60, no. 4, pp. 177-181, Apr. 2013.

[6] Z. Tong, A. Fischer, A. Stelzer, and L. Maurer, "Radiation performance enhancement of *E*-band antenna in package," *IEEE Trans. Compon. Packag. Manuf. Technol.,* vol. 3, no.11, pp. 1953-1959, Mar. 2013.

[7] J. Xu, Z. N. Chen, X. Qing, and W. Hong, "140-GHz TE_{20}-mode dielectric-loaded SIW slot antenna array in LTCC," *IEEE Trans. Antennas Propag.,* vol. 61, no. 4, pp. 1784-1793, Apr. 2013.

[8] Y. Zhang, S. Shi, R. Martin, and D. Prather, "High-gain linearly tapered antipodal slot antenna on LCP substrate at E-and W-bands," *IEEE Antennas Wireless Propag. Lett.*, vol. 15, pp. 1357-1360, 2016.

[9] N. Ghassemi, and K. Wu, "High-efficient patch antenna array for *E*-band gigabyte point-to-point wireless services," *IEEE Antennas Wireless Propag. Lett.*, vol. 11, pp. 1261-1264, 2012.

[10] J. Xu, Z. N. Chen, X. Qing, and W. Hong, "Bandwidth enhancement for a 60 GHz substrate integrated waveguide fed cavity array antenna on LTCC," *IEEE Trans. Antennas Propag.*, vol. 59, no. 3, pp. 826–832, Mar. 2011.

[11] K. Gong, Z. Chen, X. Qing, P. Chen, and W. Hang "Substrate integrated waveguide cavity backed wide slot antenna for 60-GHz bands," *IEEE Trans. Antennas Propag.*, vol. 60, no. 12, pp. 6023-6026, Dec. 2012.

[12] S. Cheng, H. Yousef, and H. Kratz, "79 GHz slot antennas based on substrate integrated waveguides (SIW) in a flexible printed circuit board," *IEEE Trans. Antennas Propag.*, vol. 57, no. 1, pp. 64–71, Jan. 2009.

[13] X.-P. Chen, K. Wu, L. Han, and F. He, "Low-cost high gain planar antenna array for 60-GHz band applications," *IEEE Trans. Antennas Propag.*, vol. 58, no. 6, pp. 2126-2129, Jun. 2010.

[14] Y. Miura, J. Hirokawa, M. Ando, Y. Shibuyam and G. Yoshida, "Double-layer full-corporate-feed hollow-waveguide slot array antenna in the 60 GHz band *IEEE Trans. Antennas Propag.*, vol. 59, no. 8, pp. 6023-6026, Aug. 2011.

[15] J. Xu, Z. Chen, X. Qing, and W. Hong, "A single-layer SIW slot array antenna with TE_{20} mode," in *Proc. Asia-Pac. Microw. Conf.*, Melbourne, Australia, Dec. 5-8, 2011, pp. 1330-1333.

[16] W. Han, F. Yang, and P. Yang, "Slotted substrate integrated cavity antenna using TE_{330} mode with low profile and high gain," *Electron. Lett.*, vol. 50, no. 7, pp. 488-490, 2014.

[17] W. Han, F. Yang, J. Ouyang, and P. Yang, "Low-cost wideband and high-gain slotted cavity antenna using higher-order modes formillimeter-wave application," *IEEE Trans. Antennas Propag.*, vol. 63, no. 11, pp. 4624-4631, Nov. 2015.

[18] Available online: http://www.matrixelectronics.com/products/Panasonic/megtron-6 .

[19] Available online: https://ats.net/products-technology/product-portfolio/hdi-any-layer-pcbs/.

[20] Available online: https://ats.net/products-technology/product-portfolio/hdi-microvia-pcbs /.

[21] https://www.aspocomp.com/ .

[22] N. Marcuivitz, *Waveguide Handbook*, New York, NY, USA: Pereginus, 1985.

[23] H. T. Hu, F. Chen, and Q. Chu, "A compact directional slot antenna and its application in MIMO array," *IEEE Trans. Antennas Propag.*, vol. 50, no. 2, pp. 67-69, Jan. 2014.

[24] C. Zhang, J. Zhang, and L. Li, "Triple band-notched UWB antenna based on SIR-DGS and fork-shaped stubs," *Electron. Lett.*, vol. 64, no. 12, pp. 5513-5517, Dec. 2016.

[25] H. Jin, K. Chin, W. Che, C. Chang, H. Li, and Q. Xue, "Differential-fed patch antenna arrays with low cross polarization and wide bandwidths," *IEEE Antennas Wireless Propag. Lett.*, vol. 13, pp. 1069-1072, 2014.

[26] W. Han, F. Yang, J. Ouyang, and P. Yang, "Millimeter-wave broadband transition of substrate integrated waveguide on high-to-low dielectric constant substrates," *IEEE Trans. Compon. Packag. Technol.*, vol. 3, no. 10, pp. 1764-1770, Mar. 2013.

[27] M. Mosalanejad, S. Brebels, I. Ocket, V. Volski, C. Soens, and G. Vandenbosch, "A complete measurement system for integrated antennas at millimeter wavelengths," in *Proc. 9th Europ. Conf. Antennas Propag. (EuCAP'2015)*, Lisbon, Portugal, Apr. 12-17, 2015, pp. 1-5.

[28] J. F. Xu, W. Hong, P. Chen, and K. Wu, "Design and implementation of low sidelobe substrate integrated waveguide longitudinal slot array antennas," *IET Microw. Antennas Propag.*, vol. 3, no. 5, pp. 790–797, Aug. 2009.